



1
2
3
4
5
6
7
8
9
10
11
12
13
14
15
16
17
18
19
20
21
22
23
24
25
26
27
28
29

**WAVINESS OF THE SOUTHERN HEMISPHERE WINTERTIME POLAR
AND SUBTROPICAL JETS**

by

Jonathan E. Martin¹ and Taylor Norton²

¹Department of Atmospheric and Oceanic Sciences

²Antarctic Meteorological Research Center

University of Wisconsin-Madison

Madison, WI 53706

Corr. Author: Jonathan E. Martin, jemart1@wisc.edu



ABSTRACT

30

31

32

33

34

35

36

37

38

39

40

41

42

43

44

45

46

47

48

49

The recently developed average latitudinal displacement (ALD) methodology is applied to assess the waviness of the austral winter subtropical and polar jets using three different reanalysis data sets. The analysis reveals both similarities and differences between the hemispheres with respect to aspects of the tendencies exhibited by both species of jets over the last 6 decades. As in the wintertime Northern Hemisphere, both jets in the Southern Hemisphere have become systematically wavier over the time series and the waviness of each jet evolves quite independently of the other during most cold seasons. Also, like its Northern Hemisphere equivalent, the Southern Hemisphere polar jet exhibits no trend in speed (though it is notably slower) while its poleward creep is statistically significant. In contrast to its Northern Hemisphere counterpart, the austral subtropical jet has undergone both a systematic increase in speed as well as a statistically significant poleward migration. Finally, composite differences between the waviest and least wavy seasons for each species suggest that the Southern Hemisphere's lower stratospheric polar vortex is negatively impacted by unusually wavy tropopause-level jets of either species.

KEYWORDS: Southern Hemisphere, winter, polar jet, subtropical jet, waviness



50 **1. Introduction**

51

52 Consideration of changes in the behavior of the tropopause-level jet streams in a warming
53 world has been catalyzed by the construction of long-period reanalysis data sets over the past
54 three decades (Kalnay et al, 1996; Kistler et al., 2001; Kobayashi et al. 2015; Copernicus
55 Climate Change Services [CS3], 2017). Recent analyses employing these data sets (e.g. Archer
56 and Caldiera, 2008; Barnes and Screen, 2015; Gallego et al. 2005; Manney and Hegglin, 2018;
57 Peña-Ortiz et al. 2013; Vavrus et al. 2017), in tandem with a number of studies based upon
58 climate model output (e.g. Barnes and Polvani, 2013; Lorenz and DeWeaver, 2007; Miller et al.
59 2006; Yin, 2005), have produced a consensus view that poleward displacement of both jets
60 accompanies warming. Along with an interest in latitudinal position, nearly all of the
61 aforementioned studies have also addressed either observed and/or forecasted changes in the
62 speed of the jet streams.

63 In a recent paper Martin (2021) offered a feature-based analysis of the *waviness* of the
64 tropopause-level polar and subtropical jets during Northern Hemisphere winter (DJF). The
65 analysis proceeded from the results of Christenson et al. (2017) that identified the isentropic
66 layers that house the two species of jets during NH winter. He found that 1) the polar jet (POLJ)
67 has undergone a statistically significant poleward migration over the time series, not matched by
68 the subtropical jet (STJ), and 2) neither jet species exhibited a trend in its speed. Additionally,
69 the analysis showed that both jets have become systematically wavier over the last 6 decades.

70 By virtue of its land/sea distribution, enhanced lower tropospheric warming at high
71 latitudes of the NH, known as Arctic amplification, has recently emerged as a prominent signal
72 of climate change (e.g., Serreze et al. 2009; Screen and Simmonds, 2013: and references therein).
73 Francis and Vavrus (2012) were among the first to propose that changes in the undulatory nature



74 of the jet stream might be linked to Arctic amplification. This suggestion initiated a decade-long
75 debate on this issue (e.g. Barnes, 2013; Blackport and Screen, 2020; DiCapua and Coumou,
76 2016; Francis, 2017; Francis and Vavrus, 2015; Francis et al. 2018; Martineau et al. 2017, Screen
77 and Simmonds, 2013; Vavrus, 2018). As noted by Martin (2021), at least some of the
78 controversy and attendant lack of consensus surrounding this question (Barnes and Polvani,
79 2015) was nourished by the absence of a robust method of assessing the waviness of the
80 tropopause-level jets. The average latitudinal displacement (ALD) methodology introduced in
81 Martin (2021) (briefly described later) offers one possible remedy to this deficiency.

82 To our knowledge, a study by Gallego et al. (2005) is the only one to consider aspects of
83 the waviness of the austral winter jets. They employed an objective method focused on
84 identifying the geostrophic streamline of maximum average velocity at 200 hPa (i.e. the jet core
85 at that level) to separately consider the behaviors of the STJ and POLJ. This method allowed
86 consideration of the jets as continuous features around the hemisphere and thus enabled a
87 number of novel analyses of their behavior and trends. With particular relevance to the present
88 study, they considered a zonal index computed as the difference between the maximum and
89 minimum latitude of the jet core (i.e. the streamline at the core of the jet) on each day. A similar
90 metric, termed DayMaxMin, was employed by Barnes (2013) in her consideration of the
91 behavior of the NH 500 hPa flow. Though insightful, such a metric does not comprehensively
92 account for the waviness created by the full collection of troughs and ridges around the
93 hemisphere that routinely characterizes the jets.

94 In this paper we apply the methodology of Martin (2021) to assess recent trends in the
95 waviness of the SH wintertime polar and subtropical jets. The method of identifying the austral
96 winter polar and subtropical jet locations in isentropic space is described in Section 2 along with



97 a description of the data sets used. Also included there is a short description of the method of
98 assessing waviness introduced in Martin (2021). In Section 3, elements of the long-term trend
99 and interannual variability of the waviness of the austral winter polar and subtropical jets are
100 presented along with differences between composites of the waviest and least wavy seasons for
101 each species. A summary and conclusions are offered in Section 4.

102

103 **2. Data and Methodology**

104

105 In the foregoing analysis, the zonal (u) and meridional (v) winds as well as temperature (T),
106 at 6 h intervals from three different reanalysis data sets are employed. 72 austral winters (JJA)
107 (1948-2019) of the National Centers for Environmental Prediction/National Center for
108 Atmospheric Research (NCEP/NCAR) reanalysis, at 17 isobaric levels to 10 hPa on a 2.5°
109 latitude-longitude grid (Kalnay et al., 1996; Kistlet et al., 2001) are used. We employ 62 winters
110 (1958-2019) of the Japanese 55-year (JRA-55) reanalysis with data on 60 vertical levels up to 0.1
111 hPa on a horizontal grid mesh of ~ 55 km (Kobayashi et al., 2015). Finally, the ERA5 reanalysis
112 data set on 137 vertical levels from the surface to 80 km with a grid spacing of 31 km covering
113 the period from 1979 to 2019 (Copernicus Climate Change Service [CS3], 2017) are used as
114 well. The waviness of the jets is assessed in the context of understanding their relationships to
115 the horizontal gradient of potential vorticity (PV) in prescribed isentropic layers. The first step
116 in the analysis, therefore, involves identification of the isentropic layers that house the austral
117 winter jets. This was accomplished empirically by identifying the isentropic level at which the
118 maximum wind speed was observed in each grid column (between 10 and 80° S) at each analysis
119 time in JJA over the 62-year time series of the JRA-55 data set. Of the three data sets employed



120 in the present work, the JRA-55 was chosen for this preliminary analysis step because both its
121 length of time series as well as its horizontal and vertical resolutions are between those
122 characterizing the other two data sets employed here. Following Koch et al. (2006) we only
123 considered columns in which the integral average wind speed exceeded 30 ms^{-1} in the 100-400
124 hPa layer. The resulting distribution is clearly tri-modal with frequency maxima, and therefore
125 separate jet features, approximately located in the 305-320, 340-355, and 395-410K isentropic
126 layers (Fig. 1a). The latter isentropic layer appears in the lower stratosphere and is associated
127 with the austral polar night jet (PNJ), which, being located *above* the tropopause, is not a focus
128 of the present analysis. Further separation of the STJ and POLJ is achieved through reference to
129 Fig. 2 of Gallego et al. (2005) which strongly implies that the STJ sharply peaks near 30°S while
130 the POLJ more broadly peaks around 50°S . Accordingly, we further constrained the analysis to
131 latitude bins $0\text{-}40^{\circ}\text{S}$ for the STJ and 40 to 65°S for the POLJ. With this additional refinement,
132 the analysis identifies the STJ in the 340-355K isentropic layer and the POLJ in the 310-325K
133 isentropic layer (Fig. 1b). Similar analyses of the other two data sets (not shown) revealed the
134 robustness of this result. It is important to note that 53.8% of all qualifying columns (to 380K) in
135 the $0\text{-}40^{\circ}\text{S}$ bin (STJ) were in the 340-355K layer while 46.8% of all qualifying columns in the
136 $40\text{-}65^{\circ}\text{S}$ bin (POLJ) were in the 310-325K layer. It is immediately apparent, consistent with
137 prior analyses (e.g. Bals-Elsholz et al. 2001, Nakamura and Shimpo 2004, Gallego et al. 2005),
138 that the STJ is the dominant jet feature in the southern winter.

139 The analysis method to be used here involves assessment of the circulation which
140 requires calculation of contour length. As a result, fair comparison among the different data sets
141 requires adoption of a uniform grid spacing. Consequently, all three data sets were bilinearly
142 interpolated onto isentropic surfaces at 5K intervals (from 280 to 380K) and 2.5° latitude-



143 longitude grid spacing using programs within the General Meteorological Analysis Package
144 (GEMPAK) (desJardins et al., 1991). The average PV and average zonal and meridional wind
145 speeds in both the polar jet (310:325K) and subtropical jet (340:355K) layers were then
146 calculated from the four times daily data for each day in each of the three time series.
147 As reviewed in Martin (2021), consideration of the quasi-geostrophic potential vorticity
148 (QGPV), following Cunningham and Keyser (2004), demonstrates that local maxima in the
149 cross-flow gradient of QGPV are collocated with maxima in the geostrophic wind speed. In the
150 Southern Hemisphere, the jets lie on the high PV edge of this PV gradient. By searching through
151 daily average isertels from -0.5 to -5.0 at 0.1 PVU intervals ($1 \text{ PVU} = 10^{-6} \text{ m}^2 \text{ K kg}^{-1} \text{ s}^{-1}$), the
152 analysis identifies a “core isertel” along which the circulation per unit length (i.e. average speed)
153 is maximized in the separate POLJ (310:325K) and STJ (340:355K) isentropic layers for every
154 day in each of the time series. This core isertel is, by design, an analytical proxy for the jet core.
155 A glimpse into the fidelity of this method in identifying the meandering cores of the POLJ and
156 STJ jets is illustrated in Fig. 2. In each case the objectively identified core isertel, in black, lies
157 very near, or at, the center of the analyzed isotach maxima around the hemisphere with
158 physically defensible exceptions. For instance, the red dashed lines in Fig. 2b indicate portions
159 of the bold black line in Fig. 2d (i.e. the overlying STJ core) suggesting that those portions of the
160 isotach maxima in Fig. 2b that are somewhat removed from the POLJ core isertel are the lower
161 portions of the overlying STJ core. Similarly, an extensive isotach maxima region in Fig. 2d has
162 a blue dashed line, a portion of the bold black line in Fig. 2b, slicing through it. This region,
163 well poleward of the STJ core isertel, is clearly the upper portion of the underlying POLJ core.
164 The waviness of each jet is assessed by calculating a hemispheric average of the meridional
165 displacements of the core isertel from its equivalent latitude – the northern extent of a polar cap



166 whose area is equal to the area enclosed by the core isertel. This metric is referred to as the
167 average latitudinal displacement (ALD). The method does not require that the core isertel be the
168 same in both jet layers on a given day, nor that it be the same from day-to-day in a given jet
169 layer. Consequently, it is important to examine its distribution in each jet layer over the entire
170 time series. Figure 3 portrays the frequency of occurrence of the core isertels in both the STJ
171 and POLJ layers for each of the three time series. The frequency of occurrence in the several
172 isertelic bins for each species of SH jet match quite well with what Martin (2021) found for the
173 NH wintertime jets, even when accommodating for the different isentropic layer for the austral
174 POLJ.

175

176 **3. Analysis**

177

178 The JJA seasonal average latitudinal displacement (ALD) of each jet is calculated as a
179 92-day average of the daily ALD in each cold season. The results are shown in Fig. 4. It is
180 instantly clear that, as in the NH, the POLJ is wavier than the STJ and that both jets have become
181 systematically wavier over the 62-year JRA-55 time series with $p < 0.004$ for both time series (a
182 one-sided Student's t -test was employed). Interestingly, the austral winter STJ is less wavy than
183 its NH counterpart but the waviness of both has increased identically at 0.005 deg/yr. The winter
184 POLJ in the SH is, on the other hand, wavier than in the NH and is trending faster (0.017 versus
185 0.009 deg/yr) than its NH complement. Daily time series of the ALD of each jet can also be
186 examined to determine the extent to which the waviness of the two jets covaries. Figure 5
187 illustrates the POLJ and STJ daily ALDs for 1999 from each of the three data sets. The low
188 correlation between the waviness of the two species in this example year represents the rule



189 rather than the exception. All told, more than 93% of the STJ and POLJ ALD seasonal time
190 series constructed for this study are correlated with magnitudes less than 0.3. This result
191 strongly suggests that the waviness of the two species evolves independently.

192 By definition, the average wind speed along the chosen core isertel on any given day
193 represents the average jet speed for that species on that day. Time series of seasonal average jet
194 core wind speeds for the wintertime STJ and POLJ in both hemispheres are shown in Fig. 6. As
195 in the NH winter (Martin, 2021), the austral POLJ shows almost no trend in jet core speed and
196 the slight change is not statistically significant. Notably, however, the SH POLJ is $\sim 6 \text{ m s}^{-1}$
197 slower on average than its NH equivalent. Aside from the fact that the NCEP reanalysis is quite
198 different from the JRA-55 until about 1970, the austral winter STJ exhibits a robust, and
199 statistically significant (p -value < 0.001), increase in speed over the
200 JRA-55 time series – in clear contrast to its NH counterpart. It is also apparent that the SH STJ
201 is slightly weaker but less interannually variable than the NH STJ.

202 Another characteristic of interest that emerges directly from the ALD analysis method is
203 the daily value of the jet core's equivalent latitude which represents its zonally averaged
204 position. Consequently, it is straightforward to construct a time series of the seasonal average
205 equivalent latitudes of the two species of jets, shown in Fig. 7. Again, as in the NH, the
206 poleward creep of the SH POLJ is occurring three times faster than that exhibited by the STJ. In
207 contrast to the situation in the NH, however, the slight poleward displacement of the SH STJ *is*,
208 like that of the POLJ, statistically significant (p -values for the POLJ and STJ are < 0.001 and
209 0.002 , respectively). It is interesting to note that while the SH STJ is located at a roughly similar
210 latitude as the NH STJ throughout the time series, the SH POLJ is $\sim 4^\circ$ further poleward during



211 winter than the NH POLJ. Overall, a much more systematic and dramatic poleward migration of
212 the two jets has occurred over the last 6 decades in SH winter as compared to NH winter.

213 Thus far the analysis has presented elements of the seasonal average behavior of the
214 austral winter jet species. The methodology, of course, allows for evaluation of daily time series
215 of ALD as well and, in fact, such an analysis underlies the presentation in Fig. 5. Using such
216 daily time series, identification of the waviest and least wavy seasons for each jet species since
217 1979 is accomplished by summing the daily departures from calendar-day average ALD over the
218 92 days of each cold season. The list of such seasonally integrated departures from average
219 waviness for each species of jet for each reanalysis data set is shown in Table 1. From this list,
220 the 5 waviest and 5 least wavy seasons for each jet species were selected to construct composites
221 of geopotential height at several isobaric levels employing the JRA-55 data. In the foregoing
222 analysis, height differences are obtained by subtracting values associated with the composite
223 least wavy seasons from those associated with the composite waviest seasons.

224 Figure 8a shows the 500 hPa geopotential height differences between the waviest and
225 least wavy POLJ seasons. Wavy POLJ years are characterized by positive height anomalies over
226 the continent and adjacent to its east and west coasts with belts of negative anomalies in a
227 crescent stretching from southwest of Chile and then extending from the east coast of South
228 America to southern Africa toward Australia. The strongest negative height anomalies in such
229 seasons occur west of South Africa implying a slight weakening of the zonal winds just south of
230 the Cape of Good Hope. Meanwhile wavy STJ years exhibit negative composite height
231 differences in roughly the same locations as the positive composite differences just described for
232 wavy POLJ years (Fig. 8b). These composite difference patterns strengthen slightly at 250 hPa



233 (Fig. 9) suggesting an equivalent barotropic structure to the tropospheric portion of the difference
234 fields.

235 The difference fields at 50 hPa imply that the waviness of both jets exerts an
236 influence on the strength of the austral polar vortex in the lower stratosphere. The anomalous
237 height field associated with wavy POLJ years (Fig. 10a) suggests a broad, though modest,
238 anticyclonic circulation anomaly just off the pole in the Western Hemisphere. Such a
239 perturbation flow would appear to interfere with the establishment and/or persistence of strong
240 vortex flow in the same location. Wavy STJ seasons also impose a dipole of positive heights the
241 axis of which stretches from Cape Horn to East Antarctica (Fig 10b). Such a configuration
242 implies that the polar vortex is both weaker and displaced off the pole in winters with wavy
243 STJs. Thus, the analysis suggests that in winters characterized by unusually wavy jets of either
244 species, the SH polar vortex is likely weaker than normal. Further investigation of this intriguing
245 implication is the subject of ongoing work.

246

247 **4. Summary**

248

249 The analysis presented here extends the application of a method developed by Martin
250 (2021) to assess the waviness of the tropopause-level jets to analysis of the austral winter polar
251 and subtropical jets. The analysis demonstrates that both jets have become systematically wavier
252 over the past 60+ years. In addition, as in the NH, the waviness of the two species of austral
253 winter jets is largely uncorrelated suggesting little systematic influence of one on the other
254 throughout the season. Along with these similarities, there appear to be some fundamental
255 asymmetries in the behavior of the wintertime tropopause-level jets between the hemispheres.



256 The austral POLJ, like its NH counterpart, has exhibited no trend in its average speed over the
257 time series, though it is notably slower than its NH wintertime equivalent. The STJ, on the other
258 hand, has roughly the same speed as that in the NH winter but, unlike its NH counterpart, has
259 undergone a systematic, statistically significant increase in its core speed since ~1960.
260 Additionally, as opposed to the situation in the NH where only the POLJ migration toward to
261 pole is statistically significant, *both* SH jets exhibit a significant poleward creep with the POLJ
262 encroachment occurring at ~3x the rate of that characterizing the STJ.

263 Finally, circulation differences between the waviest and least wavy POLJ and STJ
264 seasons are manifest in both the troposphere and lower stratosphere. In the troposphere the
265 signals are not as coherent in the SH as they were revealed to be in the NH (Martin 2021).
266 Interestingly, the analysis implies that when either the POLJ or STJ is wavier than normal in a
267 given winter, the lower stratospheric polar vortex is negatively impacted. Again, this is different
268 from the behavior of the NH polar vortex in the face of extremes in waviness.

269 The results presented here, combined with those in Martin (2021), demonstrate that in
270 both hemispheres a wavier than normal STJ during winter serves to weaken the lower
271 stratospheric polar vortex. Though, as suggested by the analysis supporting Fig. 5, the STJ and
272 POLJ do not appear to influence one another systematically, there are still instances in which the
273 waviness of the two jets can be phased so as to promote intense interactions. Daily perusal of
274 hemispheric synoptic maps suggests that such instances of jet interaction often lead to intense
275 lower tropospheric cyclogenesis events. The polar vortex can be weakened by the absorption of
276 vertically propagating planetary waves originating from such developments (Matsuno, 1971).
277 Thus, intense cyclogenesis, encouraged by wavy and well phased POLJ and STJs, may underlie
278 the association, revealed here, between tropopause-level jet waviness and polar vortex strength



279 during austral winter. Current research is examining whether such jet interaction-induced
280 cyclogenesis events from specific seasons systematically correspond to episodes of polar vortex
281 weakening.

282

283 **COMPETING INTERESTS:** The contact author has declared that none of the authors has any
284 competing interests.

285

286 **AUTHOR CONTRIBUTIONS:** J. Martin completed the ALD analysis and did all the writing,
287 figure drafting and preparation of the manuscript for submission. T. Norton performed the
288 analysis that determined the POLJ and STJ isentropic housings during SH winter.

289

290 **ACKNOWLEDGEMENTS:** This work was supported by the National Science Foundation under
291 grants ATM-1640055 and NSF-2055667. JRA-55 data available from the Research Data
292 Archive at the National Center for Atmospheric Research. The authors would like to thank Prof.
293 Andrea A. Lopez-Lang for helpful comments and suggestions.



294

REFERENCES

295

296 Archer, C. L., and K. Caldeira, 2008: Historical trends in the jet stream. *Geo. Res. Let.*, **35**(8).

297

298 Bals-Elsholz, T. M., E. H. Atallah, L. F. Bosart, T. A. Wasula, M. J. Cempa, and A. R. Lupo,
299 2001: The wintertime Southern Hemisphere split jet: Structure, variability, and evolution.
300 *J. Climate*, 14, 4191-4215.

301

302 Barnes, E. A., 2013: Revisiting the evidence linking Arctic amplification to extreme weather in
303 midlatitudes. *Geophys. Res. Let.*, **40**, 4734-4739.

304

305 _____, and L. Polvani, 2013: Response of the midlatitude jets, and of their variability, to
306 increased greenhouse gases in the CMIP5 models. *J. Climate*, 26, 7117-7135.

307

308 _____, and J. A. Screen, 2015: The impact of Arctic warming on the midlatitude jet-stream: Can
309 it? Has it? Will it? *WIREs Clim Change*, **6**, 277–286. doi: 10.1002/wcc.337.

310

311 Blackport, R., and J. A. Screen, 2020: Insignificant effect of Arctic amplification on the
312 amplitude of midlatitude atmospheric waves. *Science advances*, 6(8), p.eaay2880.

313

314 Christenson, C. E., J. E. Martin, and Z. J. Handlos, 2017: A synoptic-climatology of Northern
315 Hemisphere, cold season polar and subtropical jet superposition events. *J. Climate*, **30**,
316 7231-7246.



317

318 Copernicus Climate Change Service (C3S) (2017): ERA5: Fifth generation of ECMWF

319 atmospheric reanalyses of the global climate. Copernicus Climate Change Service

320 Climate Data Store (CDS), *March 2020*, <https://cds.climate.copernicus.eu/cdsapp#!/home>

321

322 Cunningham, P., and D. Keyser, 2004: Dynamics of jet streaks in a stratified quasi-geostrophic

323 atmosphere: Steady-state representations. *Quart. J. Roy. Meteor. Soc.*, **130**, 1579-1609.

324

325 desJardins, M. L., K. F. Brill, and S. S. Schotz, 1991: GEMPAK 5 Part I—GEMPAK 5

326 programmer's guide. National Aeronautics and Space Administration. [Available from

327 Scientific and Technical Information Division, Goddard Space Flight Center,

328 Greenbelt, MD 20771.].

329

330 DiCapua G., and D. Coumou, 2016: Changes in the meandering of the Northern Hemisphere

331 circulation. *Environ. Res. Lett.*, **11**, 094028, doi:10.1088/1748-9326/11/9/094028.

332

333 Francis, J. A., 2017: Why are Arctic linkages to extreme weather still up in the air?. *Bull. Amer.*

334 *Meteor. Soc.*, **98**, 2551-2557.

335

336 _____, and S. J. Vavrus, 2012: Evidence linking Arctic amplification to extreme weather in mid-

337 latitudes. *Geophys. Res. Lett.*, **39**, L06801, doi:10.1029/2012GL051000.

338

339 _____, and _____, 2015: Evidence for a wavier jet stream in response to rapid Arctic warming.

340 *Environ. Res. Lett.* **10**, 014005, doi:10.1088/1748-9326/10/1/014005.



341

342 _____, N. Skific, and S. J. Vavrus, 2018: North American weather regimes are becoming more

343 persistent: Is Arctic amplification a factor? *Geophys Res.Lett.*,

344 <https://doi.org/10.1029/2018GL080252>.

345

346 Gallego, D., P. Ribera, R. Garcia-Herrera, E. Hernandez, and L. Gimeno, 2005: A new look for

347 the Southern Hemisphere jet stream. *Climate Dyn.*, **24**, 607-621.

348

349 Kalnay, E. and co-authors, 1996: The NCEP/NCAR 40-year reanalysis project. *Bull. Amer.*

350 *Meteor. Soc.*, **77**, 437-470.

351

352 Kistler, R. and co-authors, 2001: The NCEP-NCAR 50-Year reanalysis: Monthly means CD-

353 ROM and documentation. *Bull. Amer. Meteor. Soc.*, **82**, 247-267.

354

355 Kobayashi, S., Y. Ota, Y. Harada, A. Ebita, M. Moriya, H. Onoda, K. Onogi, H. Kamahori, C.

356 Kobayashi, H. Endo, K. Miyaoka, and K. Takahashi, 2015: The JRA-55 reanalysis:

357 General specifications and basic characteristics. *J. Meteor. Soc. Japan*, **93**, 5-48.

358

359 Koch, P., H. Wernli, and H. C. Davies, 2006: An event-based jet-stream climatology and

360 typology. *Int. J. Climatology*, **26**, 283-301.

361

362 Lorenz, D. J., and E. T. DeWeaver, 2007: Tropopause height and zonal wind response to global

363 warming in the IPCC scenario integrations. *J. Geophys. Res: Atmos.*, **112**(D10).



364

365 Manney, G. L., and M. I. Hegglin, 2018: Seasonal and regional variations of long-term changes
366 in upper-tropospheric jets from reanalyses. *J. Climate*, **31**, 423-448.

367

368 Martin, J. E., 2021: Recent trends in the waviness of the Northern Hemisphere wintertime polar
369 and subtropical jets. *JGR Atmos.*, <https://doi.org/10.1029/2020JD033668>.

370

371 Martineaux, P., G. Chen, and D. A. Burrows, 2017: Wave events: Climatology, trends, and
372 relationship to Northern Hemisphere blocking and weather extremes. *J. Climate*, **30**,
373 5675-5697.

374

375 Matsuno, T., 1971: A dynamical model of the stratospheric sudden warming. *J. Atmos. Sci.*, **28**,
376 1479-1494.

377

378 Miller, R. L., G. A. Schmidt, and D. T. Shindell, 2006: Forced annular variations in the 20th
379 century Intergovernmental Panel on Climate Change Fourth Assessment Report models.
380 *J. Geophys. Res.*, **111**, D18101, doi:10.1029/2005JD006323.

381

382 Nakamura, H., and A. Shimpo, 2004: Seasonal variations in the Southern Hemisphere storm
383 tracks and jet streams as revealed in a reanalysis data set. *J. Climate*, **17**, 1828-1844.

384

385 Peña-Ortiz, C., D. Gallego, P. Ribera, P. Ordonez, and M. D. C. Alvarez-Castro, 2013: Observed



386 trends in the global jet stream characteristics during the second half of the 20th century,

387 *J. Geophys. Res. Atmos.*, **118**, 2702–2713, doi:10.1002/jgrd.50305.

388

389 Screen, J. A., and I Simmonds, 2013: Exploring links between Arctic amplification and mid-

390 latitude weather. *Geophys. Res. Lett.*, <https://doi.10.1002/grl.50174>.

391

392 Serreze, M.C., A. P. Barrett, J. C. Stroeve, D.N Kindig. and M.M. Holland, 2009: The

393 emergence of surface-based Arctic amplification. *Cryosphere*, **3**, 11-19.

394

395 Vavrus, S. J., 2018: The influence of Arctic amplification on mid-latitude weather and climate.

396 *Curr. Clim. Change. Rep.*, **4**, 238-249.

397

398 _____, F. Wang, J. E. Martin, J. A. Francis, Y. Peings, and J. Cattiaux, 2017: Changes in North

399 American circulation and extreme weather: Influence of arctic amplification and

400 Northern Hemisphere snow cover. *J. Climate* , **30**, 4317-4333.

401

402 Yin, J. H., 2005: A consistent poleward shift of the storm tracks in simulations of 21st century

403 climate. *Geophys. Res. Lett.*, **32**, L18701,doi:10.1029/2005GL023684.

404



	<i>POLJ</i>			<i>STJ</i>		
	<i><u>NCEP</u></i>	<i><u>JRA-55</u></i>	<i><u>ERA5</u></i>	<i><u>NCEP</u></i>	<i><u>JRA-55</u></i>	<i><u>ERA5</u></i>
1979	-45.416403	-19.684881	-64.232707	-3.7754167	11.1345645	0.70639878
1980	-59.380403	-58.393881	-63.657707	-3.2564167	4.47656452	-0.8576012
1981	18.8845972	36.4021194	21.8872927	-4.4154167	5.17956452	-2.2326012
1982	-24.813403	3.63785707	-15.198707	41.2785833	16.1355645	10.5773988
1983	-16.281403	35.8650731	-15.658707	-18.131417	-10.037435	-21.992601
1984	-14.954403	4.06711936	-6.9887073	15.8335833	19.8715645	11.5133988
1985	4.02659722	10.3371194	-20.535707	54.3615833	38.7185645	21.4393988
1986	24.2525972	43.6271194	20.5902927	-6.9904167	0.00256452	-10.285601
1987	62.9565972	77.0631194	16.8692927	-8.9194167	0.57256452	-9.2566012
1988	-2.5614028	-7.4278806	-35.518707	-1.9554167	2.34556452	-5.2936012
1989	-33.646403	9.93808658	-16.752707	35.2235833	29.6575645	19.4843988
1990	21.8045972	40.1761194	5.93129268	28.6225833	8.32356452	-0.0366012
1991	98.1615972	104.846187	79.9922927	15.9005833	13.6185645	10.0163988
1992	-31.301403	-26.480881	-43.682707	23.9145833	30.1255645	22.5733988
1993	45.9685972	64.4221194	23.6692927	-5.4784167	7.54756452	-0.9296012
1994	-29.454403	-32.656881	-69.886707	51.5895833	30.9815645	21.4813988
1995	-22.226403	-20.908881	-47.179707	-5.1054167	-12.989435	-16.721601
1996	80.0555972	96.1361194	86.8222927	-2.3444167	-10.092435	-11.395601
1997	68.8895972	57.665297	78.5282927	2.23058333	-8.3644355	-11.693601
1998	-27.166403	-32.68934	-70.988707	18.5915833	-2.3754355	-7.9706012
1999	36.1115972	-22.593881	-44.562707	3.60158333	-23.970435	-32.015601
2000	57.1715972	17.3883325	16.0832927	49.9395833	18.8905645	12.2183988
2001	51.6315972	26.2991194	8.28429268	46.9905833	7.20656452	1.48939878
2002	30.0675972	35.9181194	21.4212927	65.2545833	47.0115645	40.0813988
2003	70.6935972	52.1291194	24.5692927	12.5915833	-3.7804355	-11.507601
2004	27.8395972	-18.835881	-31.660707	39.5535833	19.0855645	13.4163988
2005	48.0095972	26.0351194	-2.9987073	-10.510417	-21.297435	-26.212601
2006	76.9665972	27.7838267	24.9342927	29.3135833	-2.1904355	-10.139601
2007	60.9595972	55.4256292	46.9952927	38.6865833	17.2975645	14.1103988
2008	67.6425972	67.2851194	66.7882927	-4.0874167	-21.790435	-25.102601
2009	69.9215972	17.7955696	23.8622927	22.6285833	-4.6854355	-8.0676012
2010	41.5965972	13.4191194	3.93329268	31.9945833	16.0065645	11.1233988
2011	118.932597	111.764119	79.1722927	11.7745833	-5.6934355	-8.7496012
2012	38.3955972	9.84011936	-2.5287073	54.8005833	14.8235645	-1.2216012
2013	32.3355972	-0.7048806	-14.266707	67.4165833	25.3645645	13.6133988
2014	52.2325972	45.4011194	-60.736707	40.1415833	20.9895645	6.32532378
2015	65.0135972	38.0481194	18.8882927	14.6575833	1.69656452	-1.7356012
2016	51.9375972	19.3210046	15.3602927	22.3815833	2.71556452	-0.3676012
2017	15.4975972	-14.224881	-38.558707	30.2145833	2.97356452	-2.2008762
2018	70.8755972	21.0891194	3.86429268	3.15258333	-7.7994355	-11.277601
2019	68.5365972	5.97811936	-22.852707	58.1465833	21.7315645	7.09439878

TABLE 1 Integrated seasonal departures from average ALD (degrees) for polar and subtropical jets from the three reanalysis data sets employed in this work. Gray (light blue) shading represents one of the top 5 waviest (least wavy) seasons.



406

FIGURE CAPTIONS

407

408 Fig. 1 (a) Distribution of grid-column maximum wind speeds found in 5K isentropic layers from
409 10 - 80°S for every 6h analysis time in JJA from 1958-2019 from the JRA-55 reanalysis. (b) As
410 for Fig. 1a except limited to (i) grid-columns in which the integral average wind speed from 400
411 to 100 hPa exceeded 30 m s^{-1} and (ii) to latitudes 0 - 40°S for the STJ and (iii) latitudes 40 to
412 65°S for the POLJ.

413

414 Fig. 2 (a) Isotachs of the daily averaged wind speed (contoured every 10 m s^{-1} and shaded above
415 30 m s^{-1}) and the core isertel (bold black line) in the 310:325K isentropic layer on 13 July 1995
416 from the JRA-55 reanalysis data. The core isertel value is -1.3 PVU. (b) As in (a) but for 24
417 August 2001. Core isertel value is -2.0 PVU. Dashed red line indicates portion of the core
418 isertel from the overlying STJ layer (depicted in Fig. 2d). (c) As in (a) but for wind speeds and
419 core isertel in the 340:355K isentropic layer on 13 July 1995. Core isertel value is -3.6 PVU. (d)
420 As in (c) but for 24 August 2001. Core isertel value is -1.4 PVU. Dashed blue line indicates a
421 portion of the core isertel from the underlying POLJ layer (depicted in Fig. 2b). See text for
422 further explanation.

423

424 Fig. 3 Frequency of occurrence of the core isertel value for each reanalysis time series in (a) the
425 STJ layer and (b) the POLJ layer. Solid blue, red and green lines in (a) and (b) are the SH
426 distributions from the NCEP, JRA55 and ERA5, respectively. The dashed blue, red and green
427 lines are the NH distributions from the NCEP, JRA55 and ERA5 reanalyses, respectively. In (b),
428 the NH distributions are from the 315:330K layer which houses the POLJ in the boreal winter.



429 Thin blue, red and green lines in (a) and (b) indicate the peak values of the core isertel in each
430 layer from each data set. Isertel values are given in potential vorticity units (PVU,
431 $1 \text{ PVU} = 10^6 \text{ K m}^2 \text{ kg}^{-1} \text{ s}^{-1}$), and are multiplied by -1 for the NH values.

432

433 Fig. 4 Seasonal average ALD (in degrees) of the SH wintertime subtropical and polar jets for
434 each cold season in the three reanalysis time series. The polar jet values are in the three shades
435 of blue while the subtropical jet values are in the three three shades of red. The dashed black line
436 through each time series represents the trend line for each (derived from the JRA-55 time series)
437 and is significant at the 96% level. Gray lines are the boreal winter ALD analysis from Fig. 6 of
438 Martin (2021). The “YEAR” on the abscissa indicates the year in which December of that cold
439 season occurred.

440

441 Fig. 5 Time series of the daily ALD of the polar (blue lines) and subtropical (red lines) jets from
442 the (a) NCEP-Reanalysis, (b) JRA-55, and (c) ERA5 data sets for austral winter 1999. The
443 correlation between the two times series from each data set is indicated.

444

445 Fig. 6 Seasonal average U along the core isertel for the subtropical (red lines) and polar (blue
446 lines) jets from each of the three SH reanalysis data sets. The thin black lines are trend lines for
447 each time series from the JRA-55 data. Gray lines are the equivalent boreal winter U analysis
448 from Fig. 9 of Martin (2021).

449

450 Fig. 7 Time series of the seasonal average equivalent latitude of the polar (blue lines) and
451 subtropical (red lines) jets from the three different SH reanalysis data sets. The thin black lines



452 are the trend lines (from the JRA-55 data) and are significant above the 99% level for both jet
453 species. Gray lines are the boreal winter equivalent latitude analysis from Fig. 10 of Martin
454 (2021).

455

456 Fig. 8 500 hPa height differences between the composite waviest and least wavy (a) polar jet
457 and (b) subtropical jet seasons constructed from the JRA-55 reanalysis. See Table 1 for
458 identification of the specific years comprising each composite. Positive (negative) height
459 differences are in solid red (blue) lines labeled in m and contoured every 10 m (-10 m) beginning
460 at 10 m (-10 m).

461

462 Fig. 9 250 hPa height differences between the composite waviest and least wavy (a) polar jet
463 and (b) subtropical jet seasons constructed from the JRA-55 reanalysis. See Table 1 for
464 identification of the specific years comprising each composite. Positive (negative) height
465 differences are in solid red (blue) lines labeled in m and contoured every 10 m (-10 m) beginning
466 at 10 m (-10 m).

467

468 Fig. 10 50 hPa height differences between the composite waviest and least wavy (a) polar jet
469 and (b) subtropical jet seasons constructed from the JRA-55 reanalysis. See Table 1 for
470 identification of the specific years comprising each composite. Positive (negative) height
471 differences are in solid red (blue) lines labeled in m and contoured every 10 m (-10 m) beginning
472 at 10 m (-10 m).

473

474

475

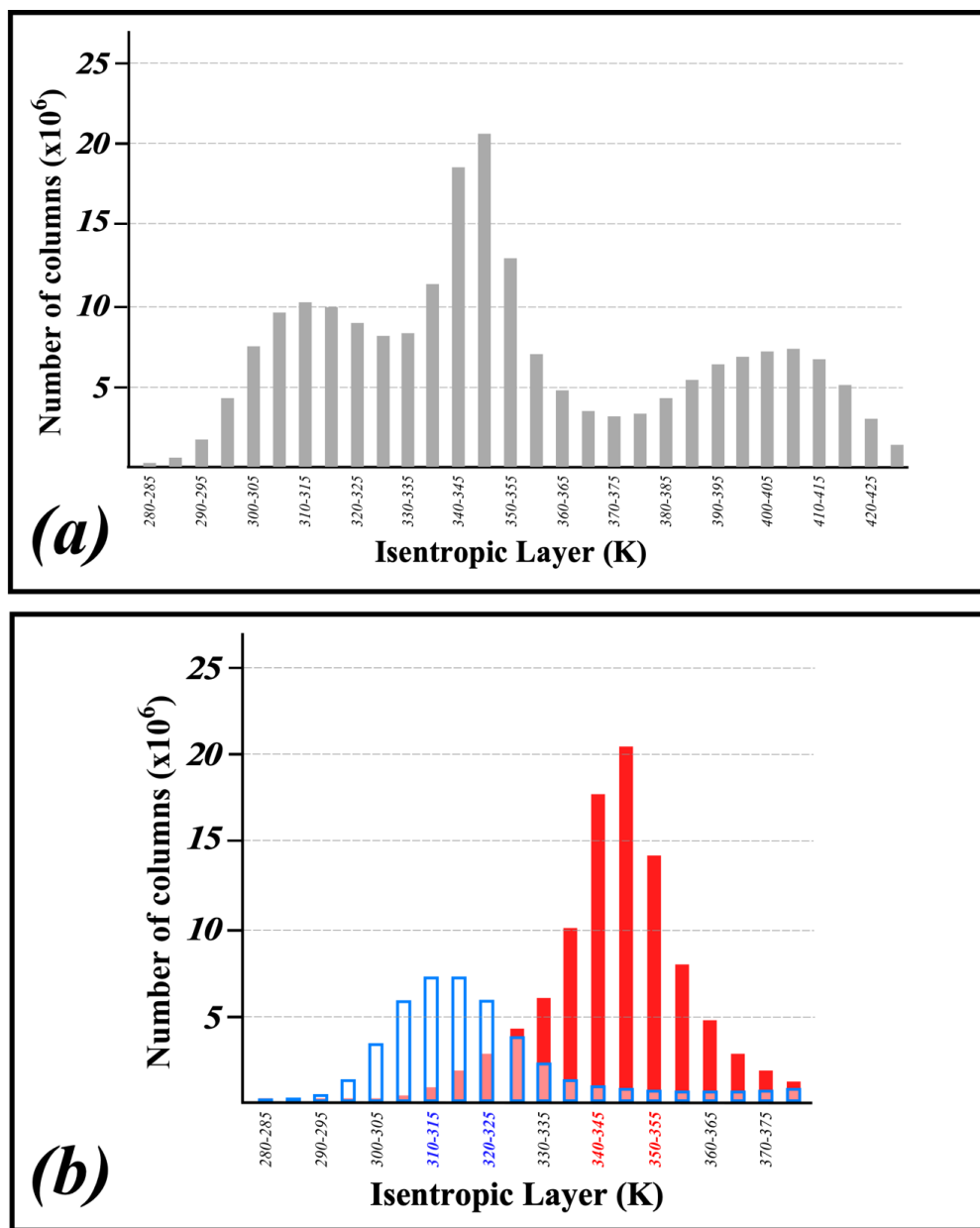


Fig. 1 (a) Distribution of grid-column maximum wind speeds found in 5K isentropic layers from 10 - 80°S for every 6h analysis time in JJA from 1958-2019 from the JRA-55 reanalysis. (b) As for Fig. 1a except limited to (i) grid-columns in which the integral average wind speed from 400 to 100 hPa exceeded 30 m s^{-1} and (ii) to latitudes 0 - 40°S for the STJ and (iii) latitudes 40 to 65°S for the POLJ.

476

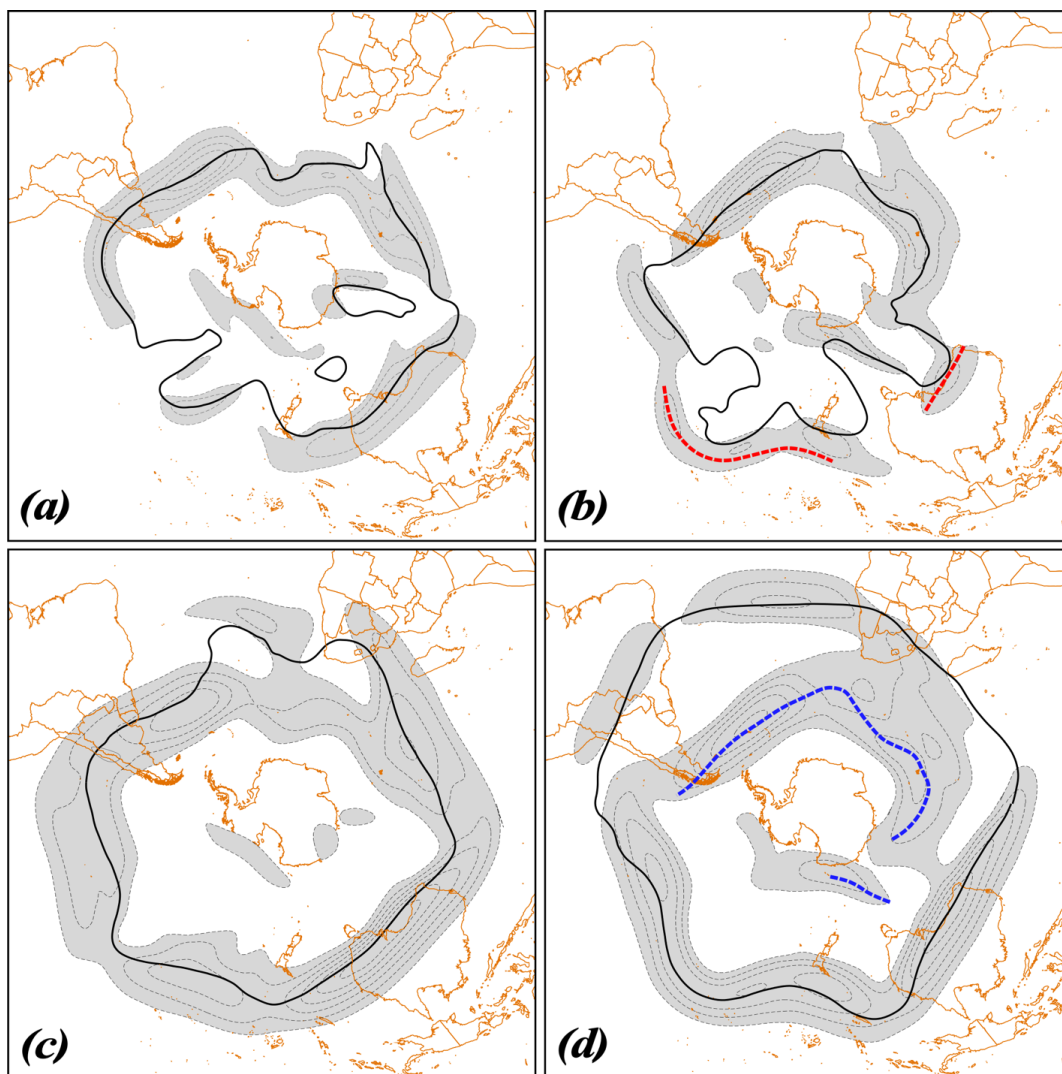


Fig. 2 (a) Isotachs of the daily averaged wind speed (contoured every 10 m s^{-1} and shaded above 30 m s^{-1}) and the core isertel (bold black line) in the 310:325K isentropic layer on 13 July 1995 from the JRA-55 reanalysis data. The core isertel value is -1.3 PVU. (b) As in (a) but for 24 August 2001. Core isertel value is -2.0 PVU. Dashed red line indicates portion of the core isertel from the overlying STJ layer (depicted in Fig. 2d). (c) As in (a) but for wind speeds and core isertel in the 340:355K isentropic layer on 13 July 1995. Core isertel value is -3.6 PVU. (d) As in (c) but for 24 August 2001. Core isertel value is -1.4 PVU. Dashed blue line indicates a portion of the core isertel from the underlying POLJ layer (depicted in Fig. 2b). See text for further explanation.

477

478

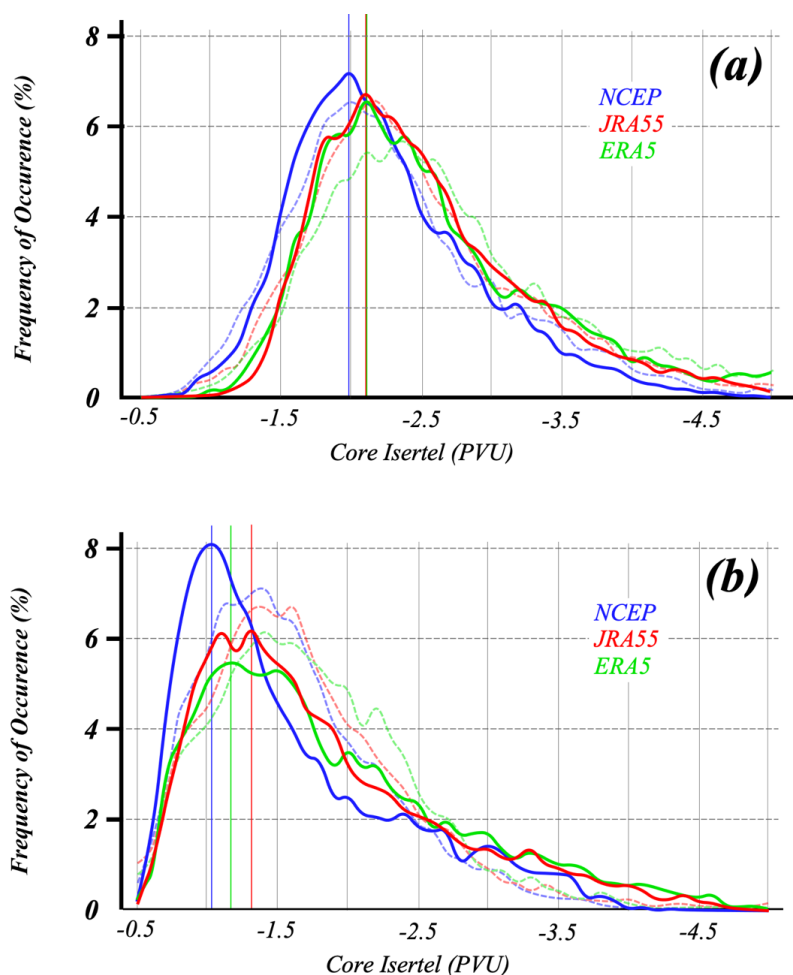


Fig. 3 Frequency of occurrence of the core isertel value for each reanalysis time series in (a) the STJ layer and (b) the POLJ layer. Solid blue, red and green lines in (a) and (b) are the SH distributions from the NCEP, JRA55 and ERA5, respectively. The dashed blue, red and green lines are the NH distributions from the NCEP, JRA55 and ERA5 reanalyses, respectively. In (b), the NH distributions are from the 315:330K layer which houses the POLJ in the boreal winter. Thin blue, red and green lines in (a) and (b) indicate the peak values of the core isertel in each layer from each data set. Isertel values are given in potential vorticity units (PVU, $1 \text{ PVU} = 10^6 \text{ K m}^2 \text{ kg}^{-1} \text{ s}^{-1}$) and are multiplied by -1 for the NH values.

479
480

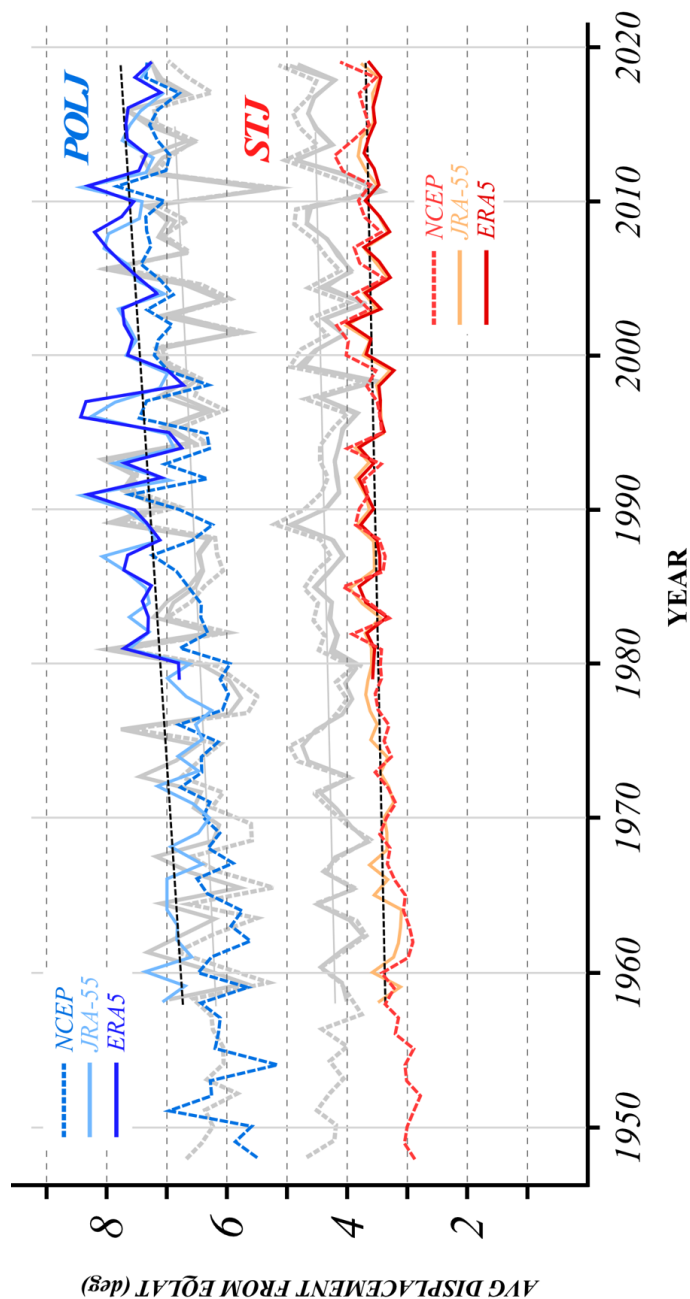


Fig. 4 Seasonal average ALD (in degrees) of the SH wintertime subtropical and polar jets for each cold season in the three reanalysis time series. The polar jet values are in the three shades of blue while the subtropical jet values are in the three shades of red. The dashed black line through each time series represents the trend line for each (derived from the JRA-55 time series) and is significant at the 96% level. Gray lines are the boreal winter ALD analysis from Fig. 6 of Martin (2021). The “YEAR” on the abscissa indicates the year in which December of that cold season occurred.

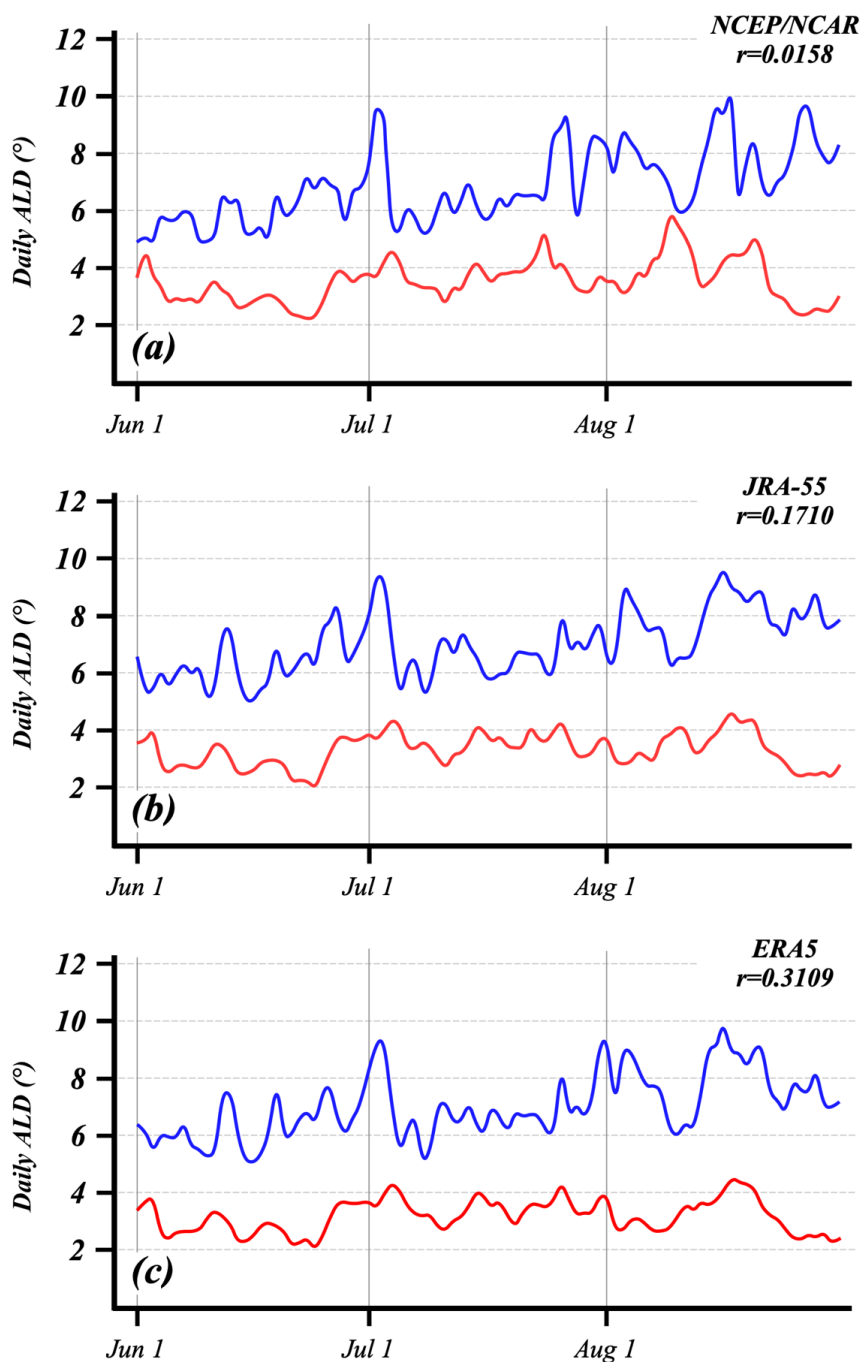


Fig. 5 Time series of the daily ALD of the polar (blue lines) and subtropical (red lines) jets from the (a) NCEP-Reanalysis, (b) JRA-55, and (c) ERA5 data sets for austral winter 1999. The correlation between the two times series from each data set is indicated.

482

483

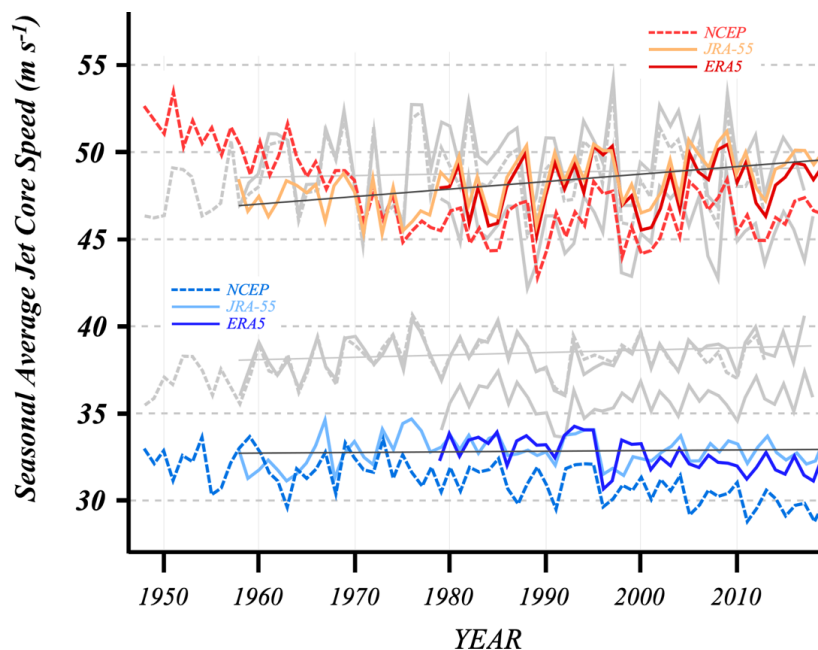


Fig. 6 Seasonal average U along the core isertel for the subtropical (red lines) and polar (blue lines) jets from each of the three SH reanalysis data sets. The thin black lines are trend lines for each time series from the JRA-55 data. Gray lines are the equivalent boreal winter U analysis from Fig. 9 of Martin (2021).

484
485

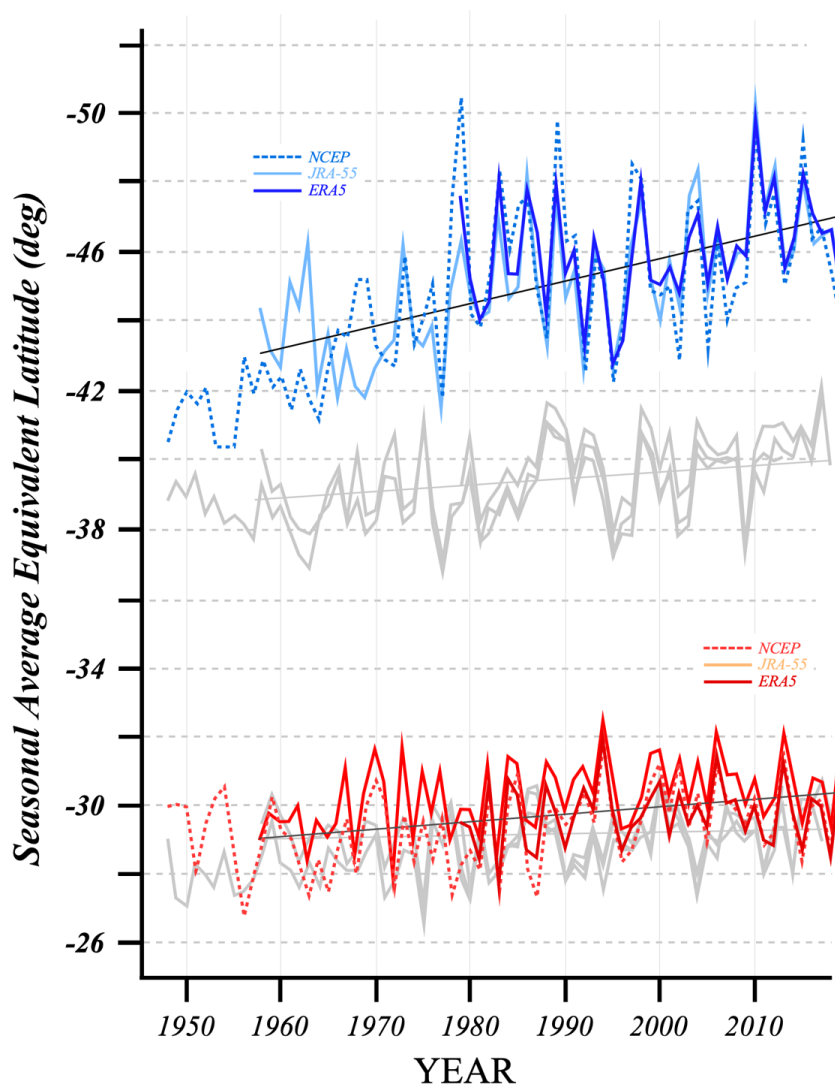


Fig. 7 Time series of the seasonal average equivalent latitude of the polar (blue lines) and subtropical (red lines) jets from the three different SH reanalysis data sets. The thin black lines are the trend lines (from the JRA-55 data) and are significant above the 99% level for both jet species. Gray lines are the boreal winter equivalent latitude analysis from Fig. 10 of Martin (2021).

486

487

488

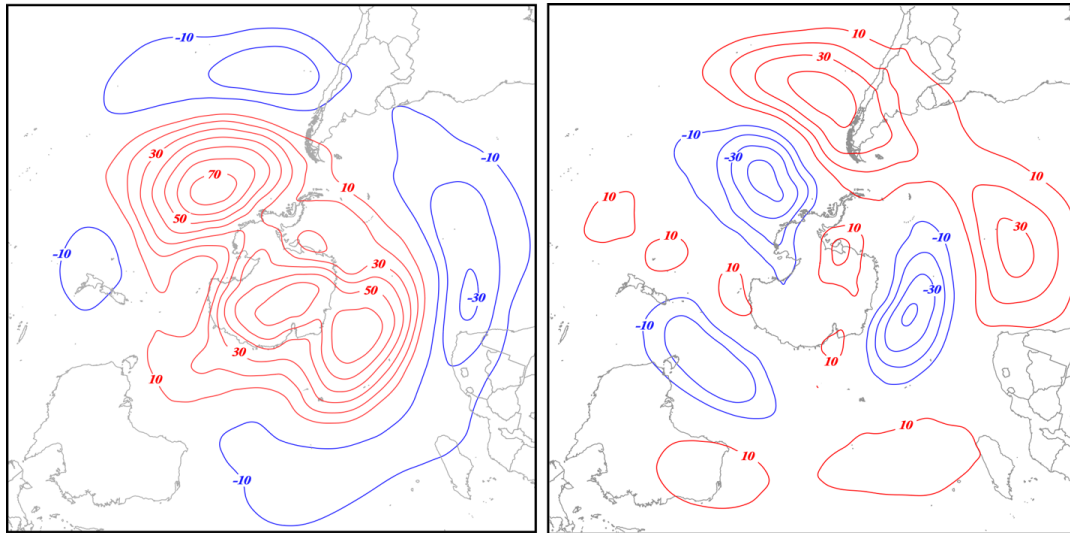


Fig. 8 500 hPa height differences between the composite waviest and least wavy (a) polar jet and (b) subtropical jet seasons constructed from the JRA-55 reanalysis. See Table 1 for identification of the specific years comprising each composite. Positive (negative) height differences are in solid red (blue) lines labeled in m and contoured every 10 m (-10 m) beginning at 10 m (-10 m).

489
490
491
492
493
494

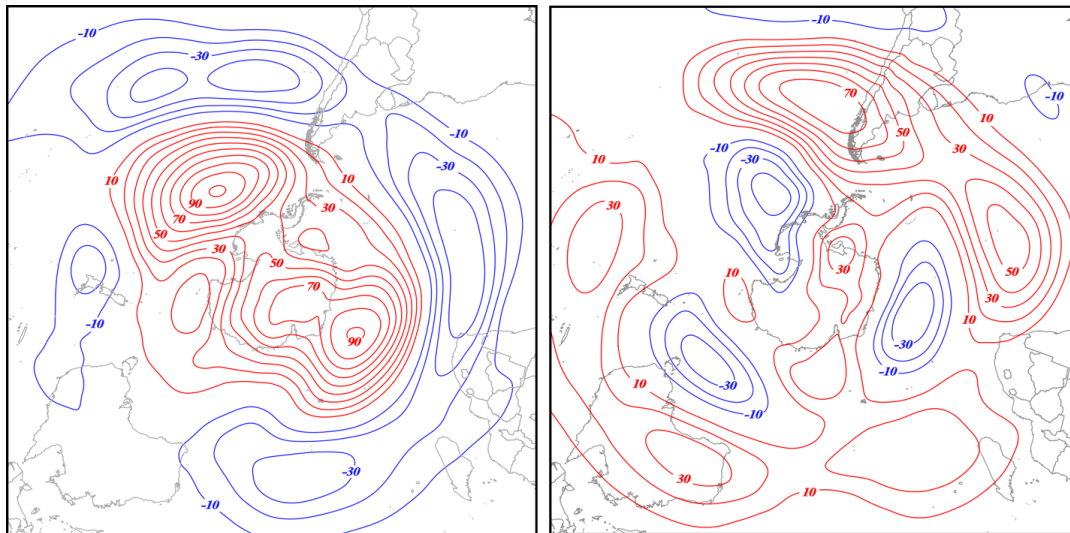
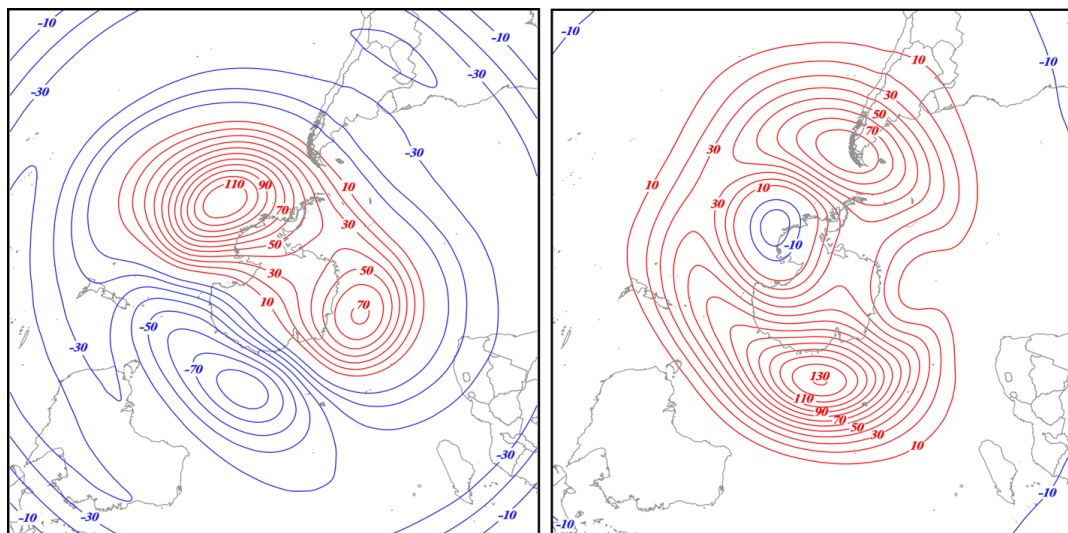


Fig. 9 250 hPa height differences between the composite waviest and least wavy (a) polar jet and (b) subtropical jet seasons constructed from the JRA-55 reanalysis. See Table 1 for identification of the specific years comprising each composite. Positive (negative) height differences are in solid red (blue) lines labeled in m and contoured every 10 m (-10 m) beginning at 10 m (-10 m).

495
496



497



498

Fig. 10 50 hPa height differences between the composite waviest and least wavy (a) polar jet and (b) subtropical jet seasons constructed from the JRA-55 reanalysis. See Table 1 for identification of the specific years comprising each composite. Positive (negative) height differences are in solid red (blue) lines labeled in m and contoured every 10 m (-10 m) beginning at 10 m (-10 m).